isolated normal NK cell samples, followed by centrifugation. The packed cell sediments were fixed in formalin for tissue processing.

RNA extraction from FFPE, NK cell lines, and normal NK cells

Total RNA from NKTL FFPE tissues and FFPE normal tissue controls was isolated using a High Pure RNA Paraffin Kit (Roche Applied Science, Mannheim, Germany) according to the manufacturer's instructions. All the sections were deparaffinized with xylene, subjected to proteinase K digestion, and RNA was extracted according to the manufacturer's protocol.

Total RNA was extracted from freshly isolated cells from NK cell lines and normal NK cell samples obtained from healthy donors using the miRNeasy Mini Kit (Qiagen GmbH, Hilden, Germany) protocol with DNaseI treatment included. The concentration and purity of the total RNA extracted were measured using a NanoDrop ND 3.0 spectrophotometer (NanoDrop Technologies Inc, Wilmington, DE, USA). RNA quality was assessed with an Agilent 2100 Bioanalyzer (Agilent Technologies, Palo Alto, CA, USA) and an RNA 6000 LabChip Kit (Agilent Technologies). Of the samples with RNA extracted, nine met the quality requirements and were used for GEP and subsequent analysis.

Gene expression profiling and analysis

GEP was performed according to the complementary DNA-mediated annealing, selection, extension, and ligation (DASL) assay (Illumina, Inc, San Diego, CA, USA) [16,17]. Raw signal intensities of each probe were obtained from data analysis software (Beadstudio; Illumina, San Diego, CA, USA). The data were normalized using a linear calibration method. Hierarchical clustering of samples was performed using the Pearson coefficient and the Ward method as the similarity and linkage methods, respectively, using the Bioconductor packages of R. To derive the NKTL-specific gene expression profiles, we extracted genes differentially expressed between NK cell lines and NKTL FFPE samples, and normal NK cells and normal FFPE controls using significance analysis of microarray (SAM) [18] (see Supporting information, Supplementary methods).

To further understand the functional and biological relevance of differentially expressed genes, gene ontology and pathway/network analysis was performed using the web-based software MetaCore (GeneGo, St Joseph, MI, USA). The software contains an interactive, manually annotated database derived from literature publications on proteins and small molecules that allows for representation of biological functionality and integration of functional, molecular, and clinical information. Several algorithms to enable both the construction and the analysis of gene networks were integrated as previously described [19]. The output p values reflect scoring, prioritization, and statistical significance of networks according to the relevance of input data.

Quantitative PCR for validation of selected genes

A reverse transcription reaction was carried out using the High Capacity cDNA Reverse Transcription Kit system (ABI, Foster City, CA, USA). Real-time fluorescent monitoring of the PCR products was performed using the Power SYBR Green PCR Master Mix (ABI) and gene-specific primers (Supporting information, Supplementary Table 4). Real-time PCR was performed in the ABI PRISM 7300 Sequence Detection system (Applied Biosystems, foster city, CA, USA) and analysed utilizing Sequence Detection Software v1.4 (ABI). Using endogenous GAPDH as an internal control for comparison, relative quantification of gene expression levels was performed and calculated using $2(-\Delta\Delta CT)$.

FISH for c-Myc translocation

MYC breakapart (BAP) probes were designed using the University of California Santa Cruz Genome Browser (http://www.genome.UCSC.edu) to identify bacterial artificial chromosomes (BACs) flanking the genes of interest (Supporting information, Supplementary Table 5). DNA was isolated (Plasmid Maxi Kit; Qiagen, Valencia, CA, USA) from BAC clones (ResGen™; Invitrogen, Carlsbad, CA, USA) and labelled with Texas Red-dUTP (Molecular Probes, Invitrogen, Carlsbad, CA, USA) or SpectrumGreen-dUTP (Abbott Molecular, Des Plaines, IL, USA). FISH was performed on TMA sections and scored as previously described [20]. Sections were analysed qualitatively by a microscopist (ML) and a minimum of 50 cells with strong FISH signals was required for a sample to be considered informative.

Terameprocol (EM-1421) treatment of NK cell lines

NK cell lines were treated with varying concentrations of the BIRC5 inhibitor Terameprocol (EM-1421; Erimos Pharmaceuticals, Houston, TX, USA) [21, 22] and control. Following incubation for 48 h, the cells were harvested, washed in PBS, and subjected to (i) MTS assay to evaluate the degree of cell viability (see Supporting information, Supplementary methods); (ii) flow cytometric analysis to assess the degree of apoptotic cell death using Annexin-V-APC and propidium iodide (PI) staining (BD Pharmigen, CA, USA); and (iii) western blot analysis to confirm successful inhibition of BIRC5 (Supporting information, Supplementary methods). The flow cytometry analysis was performed on a BD LSR II flow cytometer (Becton Dickinson, CA, USA) using BD FACSDiva™ software.

Table 1. Pathways and cellular processes enriched in genes differentially expressed between NKTL and normal NK cells

Map	Map folders	Cell process	*p* value	Objects in gene list	Objects in map
Cell cycle_The metaphase checkpoint	Congenital, Hereditary, and Neonatal Diseases and Abnormalities Regulatory processes/Cell cycle	Cell cycle	4.01E-05	10	36
Cell cycle_Chromosome condensation in prometaphase	Regulatory processes/Cell cycle	Cell cycle	1.21E-04	7	20
Cell cycle_Transition and termination of DNA replication	Regulatory processes/Cell cycle	Cell cycle	7.48E-04	7	26
Cell cycle_Start of DNA replication in early S phase	Regulatory processes/Cell cycle	Cell cycle	2.30E-03	7	31
Cell cycle_Role of APC in cell cycle regulation	Regulatory processes/Cell cycle	Cell cycle	2.79E-03	7	32
Cell cycle_Initiation of mitosis	Congenital, Hereditary, and Neonatal Diseases and Abnormalities Regulatory processes/Cell cycle	Cell cycle	3.42E-03	6	25
Cell cycle_Spindle assembly and chromosome separation	Regulatory processes/Cell cycle	Cell cycle	1.22E-02	6	32
DNA damage_ATM/ATR regulation of G2/M checkpoint	Congenital, Hereditary, and Neonatal Diseases and Abnormalities Regulatory processes/Cell cycle Regulatory processes/DNA damage	Cell cycle	1.96E-02	5	26
Transcription_Sin3 and NuRD in transcription regulation	Regulatory processes/Transcription	Transcription	2.73E-02	6	38
Cell cycle_Cell cycle (generic schema)	Congenital, Hereditary, and Neonatal Diseases and Abnormalities Regulatory processes/Cell cycle	Cell cycle	3.72E-02	4	21
Development_MAG-dependent inhibition of neurite outgrowth	Congenital, Hereditary, and Neonatal Diseases and Abnormalities Protein function/Growth factors Regulatory processes/Development/Neurogenesis	Intracellular receptor-mediated signalling pathway, response to extracellular stimulus	4.44E-02	5	32

Results

Analysis of GEP of NKTL

We compared the gene expression of NKTL FFPE samples ($n = 9$) with that of normal NK cells, as well as the respective normal FFPE tissue controls from nasal, skin and soft tissue, intestinal tract, and lymph node (see Supporting information, Supplementary methods). Among the genes showing at least a two-fold and statistically significant difference ($p < 0.05$), 339 were found to be up-regulated and 737 were down-regulated in NKTL compared with normal NK cells (Supporting information, Supplementary Table 6). We performed quantitative PCR validation on a few interesting genes frequently involved in tumour oncogenesis, including *BIRC5* (*survivin*), *EZH2*, *STMN1*, and *WHSC1*. On the whole, the quantitative PCR results were consistent with GEP data showing overexpression of *BIRC5*, *EZH2*, and *STMN1* in NK cell lines compared with normal NK cells (see the Supporting information, Supplementary Figure 1).

These differentially expressed genes were significantly enriched for cell cycle-related pathways and processes (Table 1), suggesting that NKTLs are significantly more proliferative than normal NK cells. Amongst the key proteins involved in cell cycle and mitosis are PLK1, CDK1, and Aurora-A. These proteins may also be potential therapeutic targets because of their involvement in carcinogenesis [23–25].

Using MetaCore, we found that the differentially expressed genes between NKTL and normal NK cells were enriched for targets of a number of transcription factors including Myc, p53, and NF-κB subunits (Table 2). When we further examined the expression of the Myc transcription targets and their relationship with Myc, it was striking that most of the genes up-regulated and down-regulated in our list of differentially expressed genes have been shown by previous experiments to be concordantly expressed and repressed by Myc (Figure 1A). This result suggests that Myc is activated in NKTL compared with normal NK cells. In contrast, the transcription targets of p53 in our list of differentially expressed genes showed a predominantly opposite effect to what is expected under normal p53 control, ie genes that are normally repressed by p53 were up-regulated in NKTL compared with normal NK cells, and vice versa (Figure 1B), indicating deregulation of the p53 transcription factor in NKTL compared with normal NK cells.

We further assessed the expression of a previously published NF-κB signature [26] and a validated MYC signature (unpublished) in the gene expression dataset.

Table 2. Targets of transcription targets enriched amongst genes differentially expressed between NKTL and normal NK cells

No	Network	GO processes	Total nodes	Root nodes	p value	zScore	gScore
1	c-Myc	Cell cycle (33.8%; 4.867e-13), cell division (21.1%; 2.325e-12), cell cycle process (26.8%; 4.968e-11), cell cycle phase (23.9%; 5.019e-11), mitotic cell cycle (21.1%; 5.843e-10)	73	72	3.28E-149	89.37	89.37
2	SP1	Cell division (13.8%; 2.728e-06), positive regulation of cellular process (35.4%; 3.296e-06), positive regulation of catalytic activity (18.5%; 4.041e-06), regulation of catalytic activity (23.1%; 4.731e-06), regulation of molecular function (24.6%; 4.773e-06)	65	64	2.66E-132	84.18	84.18
3	p53	Regulation of cell cycle (26.7%; 3.272e-11), cell cycle (33.3%; 5.758e-11), cell division (20.0%; 7.506e-10), cell cycle process (26.7%; 1.779e-09), cell cycle checkpoint (13.3%; 2.766e-09)	62	61	5.59E-126	82.15	82.15
4	ESR1 (nuclear)	Regulation of cell cycle (25.0%; 2.165e-08), cell division (18.8%; 1.881e-07), cell cycle checkpoint (12.5%; 4.328e-07), regulation of mitotic cell cycle (14.6%; 6.202e-07), negative regulation of cellular process (39.6%; 1.318e-06)	53	52	4.48E-107	75.73	75.73
5	CREB1	Cell cycle (31.7%; 2.639e-07), M phase (22.0%; 3.244e-07), regulation of cell cycle (24.4%; 4.238e-07), cell division (19.5%; 6.635e-07), cell cycle phase (22.0%; 4.111e-06)	42	41	4.25E-84	67.07	67.07
6	RelA (p65 NF-κB subunit)	Regulation of cell proliferation (38.9%; 2.214e-08), positive regulation of biological process (52.8%; 6.173e-08), developmental process (69.4%; 8.591e-08), biological regulation (94.4%; 8.778e-08), positive regulation of cellular process (50.0%; 8.804e-08)	38	37	8.86E-76	63.63	63.63
7	GATA-1	Cell division (22.9%; 1.798e-07), regulation of cell cycle (25.7%; 9.966e-07), M phase (22.9%; 1.068e-06), cell cycle checkpoint (14.3%; 2.108e-06), cell cycle (31.4%; 2.446e-06)	35	34	1.49E-69	60.92	60.92
8	Androgen receptor	Regulation of cell cycle (33.3%; 1.553e-08), M phase (30.0%; 1.661e-08), cell cycle (40.0%; 3.930e-08), cell division (26.7%; 4.844e-08), negative regulation of cellular process (53.3%; 5.874e-08)	33	32	2.07E-65	59.04	59.04
9	c-Fos	Biological regulation (93.8%; 8.492e-07), regulation of metabolic process (62.5%; 2.756e-06), regulation of cellular process (87.5%; 4.280e-06), regulation of cell cycle (25.0%; 5.084e-06), M phase (21.9%; 7.025e-06)	32	31	2.44E-63	58.09	58.09
10	c-Rel (NF-κB subunit)	Regulation of cell cycle (31.0%; 1.674e-07), cell cycle (34.5%; 2.717e-06), M phase (24.1%; 3.459e-06), mitotic cell cycle (24.1%; 9.697e-06), cell division (20.7%; 1.212e-05)	31	30	2.85E-61	57.11	57.11
11	HNF6	Regulation of cell cycle (31.0%; 1.674e-07), M phase (27.6%; 2.200e-07), cell cycle (37.9%; 2.788e-07), cell division (24.1%; 7.233e-07), mitotic cell cycle (27.6%; 7.253e-07)	30	29	3.33E-59	56.12	56.12
12	PPAR-gamma	Regulation of cell cycle (31.0%; 1.674e-07), cell cycle (37.9%; 2.788e-07), cell division (24.1%; 7.233e-07), mitotic cell cycle (27.6%; 7.253e-07), cell cycle checkpoint (17.2%; 7.936e-07)	29	28	3.87E-57	55.11	55.11
13	STAT3	M phase (27.6%; 2.200e-07), cell cycle (37.9%; 2.788e-07), cell division (24.1%; 7.233e-07), mitotic cell cycle (27.6%; 7.253e-07), cell cycle process (31.0%; 1.649e-06)	29	28	3.87E-57	55.11	55.11
14	E2F1	Cell division (42.9%; 2.758e-14), cell cycle (57.1%; 1.936e-13), mitotic cell cycle (42.9%; 2.870e-12), cell cycle phase (42.9%; 1.646e-11), DNA metabolic process (42.9%; 3.985e-11)	28	27	4.49E-55	54.08	54.08
15	HIF1A	Regulation of cell cycle (37.0%; 4.751e-09), negative regulation of cellular process (55.6%; 7.431e-08), cell cycle (40.7%; 1.168e-07), negative regulation of biological process (55.6%; 2.183e-07), regulation of mitotic cell cycle (22.2%; 2.953e-07)	27	26	5.19E-53	53.03	53.03
16	CDP/Cux	Cell cycle (59.3%; 8.763e-14), M phase (37.0%; 2.405e-10), mitotic cell cycle (37.0%; 1.107e-09), mitosis (29.6%; 2.891e-09), M phase of mitotic cell cycle (29.6%; 3.407e-09)	27	26	5.19E-53	53.03	53.03

Table 2. (*Continued*)

No	Network	GO processes	Total nodes	Root nodes	*p* value	zScore	gScore
17	N-Myc	Cell cycle (46.2%; 5.436e-09), cell division (30.8%; 1.378e-08), regulation of cell cycle (34.6%; 5.685e-08), mitotic cell cycle (30.8%; 2.836e-07), cell cycle checkpoint (19.2%; 4.460e-07)	26	25	5.97E-51	51.96	51.96
18	GCR-alpha	Negative regulation of cellular process (57.7%; 3.722e-08), negative regulation of biological process (57.7%; 1.105e-07), cell division (26.9%; 3.196e-07), cell cycle (38.5%; 8.437e-07), regulation of cell cycle (30.8%; 8.926e-07)	26	25	5.97E-51	51.96	51.96
19	AML1 (RUNX1)	Regulation of cell cycle (38.5%; 3.078e-09), cell cycle (46.2%; 5.436e-09), cell division (30.8%; 1.378e-08), mitotic cell cycle (34.6%; 1.544e-08), cell cycle process (38.5%; 4.140e-08)	26	25	5.97E-51	51.96	51.96
20	TCF7L2 (TCF4)	Negative regulation of cellular process (60.0%; 1.775e-08), regulation of cell cycle (36.0%; 3.824e-08), cell cycle (44.0%; 4.443e-08), negative regulation of biological process (60.0%; 5.327e-08), cell cycle process (36.0%; 3.906e-07)	25	24	6.85E-49	50.87	50.87
21	VDR	Cell division (28.0%; 2.373e-07), cell cycle (40.0%; 5.473e-07), regulation of cell cycle (32.0%; 6.354e-07), M phase (28.0%; 1.154e-06), mitotic cell cycle (28.0%; 3.281e-06)	25	24	6.85E-49	50.87	50.87
22	ATF-2	Cell cycle (40.0%; 5.473e-07), regulation of cell cycle (32.0%; 6.354e-07), M phase (28.0%; 1.154e-06), mitotic cell cycle (28.0%; 3.281e-06), cell division (24.0%; 4.806e-06)	25	24	6.85E-49	50.87	50.87
23	IRF1	Regulation of cell cycle (36.0%; 3.824e-08), cell cycle (40.0%; 5.473e-07), M phase (28.0%; 1.154e-06), mitotic cell cycle (28.0%; 3.281e-06), cell division (24.0%; 4.806e-06)	25	24	6.85E-49	50.87	50.87
24	FKHR	Cell cycle (41.7%; 3.461e-07), regulation of cell cycle (33.3%; 4.443e-07), negative regulation of cellular process (54.2%; 8.335e-07), M phase (29.2%; 8.479e-07), post-translational protein modification (45.8%; 1.468e-06)	24	23	7.83E-47	49.75	49.75
25	Brca1	Regulation of cell cycle (41.7%; 1.203e-09), cell cycle (50.0%; 1.694e-09), cell cycle checkpoint (25.0%; 5.340e-09), cell cycle process (41.7%; 1.649e-08), mitotic cell cycle (33.3%; 1.401e-07)	24	23	7.83E-47	49.75	49.75
26	RARalpha	Cell division (29.2%; 1.736e-07), cell cycle (41.7%; 3.461e-07), regulation of cell cycle (33.3%; 4.443e-07), negative regulation of cellular process (54.2%; 8.335e-07), M phase (29.2%; 8.479e-07)	24	23	7.83E-47	49.75	49.75
27	MYOD	Cell cycle (41.7%; 3.461e-07), regulation of cell cycle (33.3%; 4.443e-07), M phase (29.2%; 8.479e-07), cell differentiation (54.2%; 1.202e-06), post-translational protein modification (45.8%; 1.468e-06)	24	23	7.83E-47	49.75	49.75
28	HMGI/Y	Cell cycle (43.5%; 2.128e-07), regulation of cell cycle (34.8%; 3.046e-07), M phase (30.4%; 6.128e-07), mitotic cell cycle (30.4%; 1.754e-06), cell cycle process (34.8%; 2.387e-06)	23	22	8.91E-45	48.61	48.61
29	HOXD13	Cell division (30.4%; 1.249e-07), cell cycle (43.5%; 2.128e-07), regulation of cell cycle (34.8%; 3.046e-07), M phase (30.4%; 6.128e-07), regulation of cell proliferation (43.5%; 6.871e-07)	23	22	8.91E-45	48.61	48.61
30	PPARGC1 (PGC1-alpha)	Cell cycle (43.5%; 2.128e-07), regulation of cell cycle (34.8%; 3.046e-07), M phase (30.4%; 6.128e-07), mitotic cell cycle (30.4%; 1.754e-06), cellular biopolymer metabolic process (87.0%; 1.992e-06)	23	22	8.91E-45	48.61	48.61

Consistent with the MetaCore analysis, we observed that the MYC and NF-κB signatures were highly expressed in the NK cell lines and tumour samples compared with normal NK cells. When these two signatures were summarized into indices using the median expression of genes constituting the respective signatures, both the NF-κB index and the MYC index were significantly higher in NK cell lines and NKTL than in normal NK cells (Figure 1C).

As NKTL is an aggressive lymphoma often with extranodal involvement, we wanted to see if there was any enrichment among dysregulated genes for cell

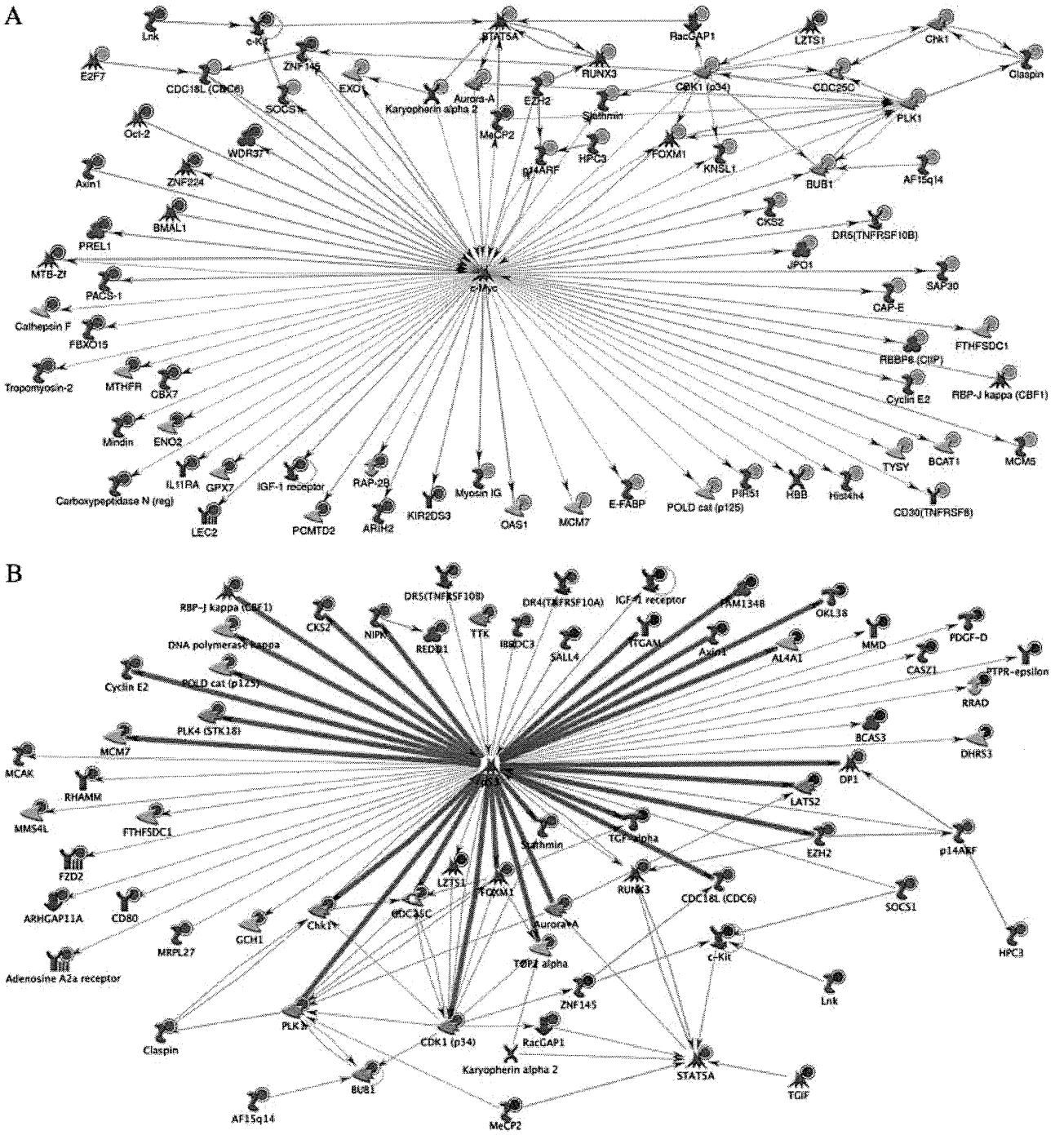

Figure 1. Gene expression profiling and networks formed by genes differentially expressed between NKTL and normal NK cells as analysed using MetaCore. (A) Network comprising transcriptional targets of MYC. Most of the transcriptional targets are expressed in concordance with the expected effect of MYC activation. (B) On the other hand, expression of transcriptional targets of p53 is discordant with the expected effect of p53 activated (interactions highlighted by magenta colour). In these figures, genes in our differentially expressed gene list (Supporting information, Supplementary Table 6) are indicated by a red circular 'target' or a blue circular 'target' to the upper right of the gene symbols if overexpressed or underexpressed, respectively. The directions of arrows connecting different molecules indicate the direction of interaction. Connecting lines in green represent a stimulating interaction and those in red an inhibitory interaction. If the line is in grey, the nature of the interaction is unknown. The different symbols signify different functions of each molecule, eg transcription factors, receptors, etc. (C) Heat map showing expression of NF-κB and MYC signatures in NK cell lines, NKTL and normal NK cells, and tissue control. Overexpressed and underexpressed genes are in red and green, respectively, with yellow indicating median expression. The dot-plot indicates that when these signatures are summarized into indices, both the NFKB and the MYC indices are significantly higher in NK cell lines and NKTL than in normal NK cells.

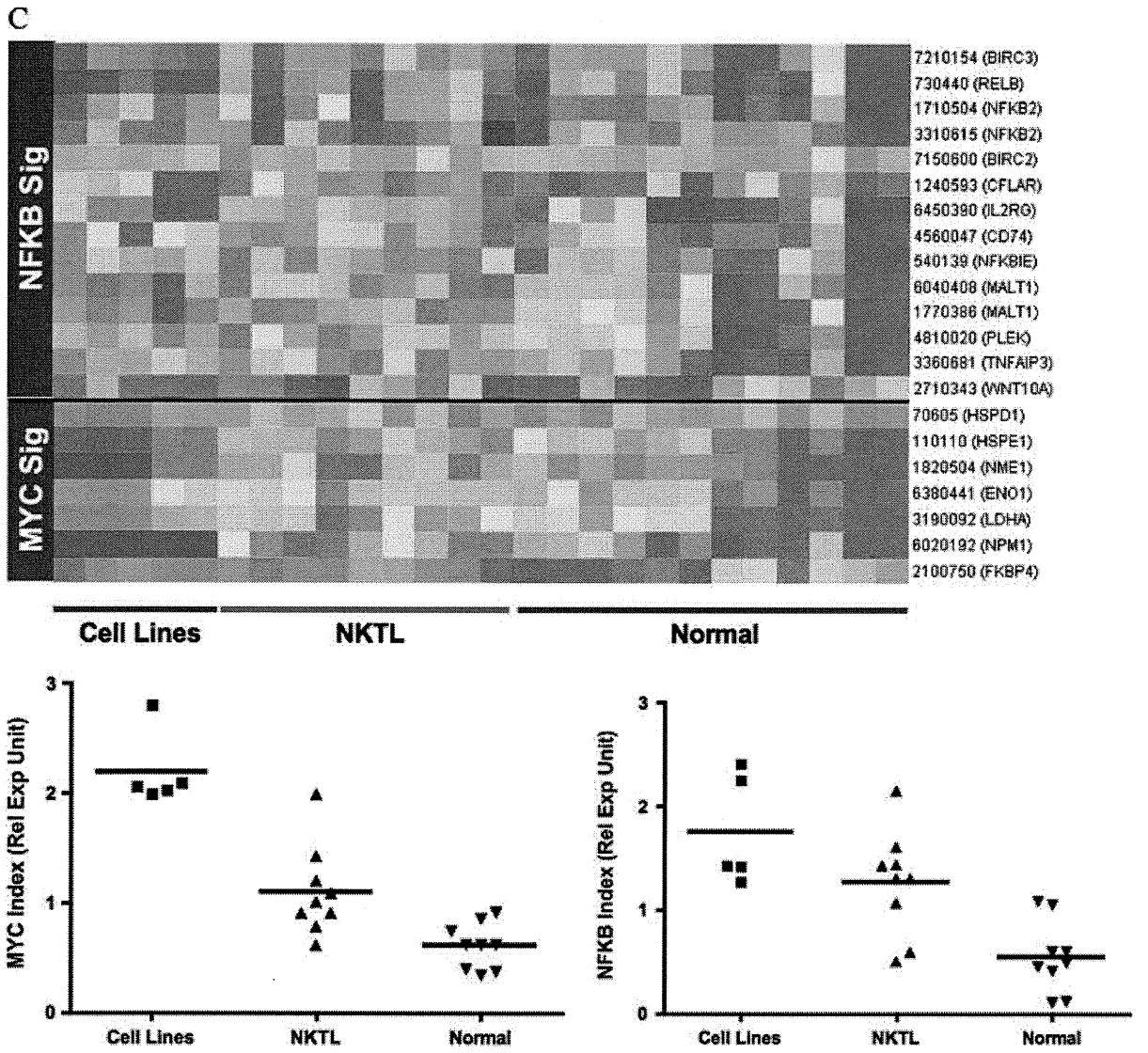

Figure 1. (*Continued*).

adhesion or metastasis-related genes. We performed Individual Pathway Activity Score Analysis (iPASA, http://lab.selfip.net/iPASA/) [27], a modification of gene set enrichment analysis, and found several metastasis-related gene sets to have higher scores in NKTL and NK cell lines than in normal NK cells (Supporting information, Supplementary Figure 2). However, an analysis of the genes contributing most significantly to the high scores of these gene sets suggested that this was predominantly due to cell cycle-related genes (Supporting information, Supplementary Figure 3).

Immunohistochemistry

To validate our gene expression results, we performed IHC for c-Myc, p53, all five subunits of the NF-κB pathway, and survivin on TMA sections containing 33 samples of NKTL. In corroboration with the GEP findings, we observed a significant percentage of our NKTL cases showing positive expression for c-Myc (15/33, 45.4%), p53 (29/33, 87.9%), NF-κB p50 (21/31, 67.7%), and survivin (32/33, 97%) (Figure 2 and Supporting information, Supplementary Table 7). Furthermore, there was a significant correlation between c-Myc immunoreactivity and the

Figure 2. Validation of gene expression profiling by IHC. (A, B) Case NKTL 23 showing nuclear expression of c-Myc in the medium and large tumour cells. (A) H&E (B) c-Myc. (C, D) Case NKTL 33 showing strong p53 nuclear staining in the neoplastic cells, which range from small to large and display irregular nuclear contours. (C) H&E (D) p53. (E, F) Strong nuclear expression for survivin observed in the medium and large neoplastic lymphocytes in case NKTL 32. (E) H&E (F) survivin. (G, H) Case NKTL 9 with positive nuclear and cytoplasmic staining for p50 in the small neoplastic lymphocytes. Only nuclear expression is regarded as constitutive p50 activation. (G) H&E (H) p50. (I, J) Moderate to strong nuclear and cytoplasmic immunoreactivity for RelB in the large pleomorphic lymphoid cells of case NKTL 6. (I) H&E (J) RelB. All photographs were taken with a DP20 Olympus camera (Olympus, Tokyo, Japan) using an Olympus BX41 microscope (Olympus). Images were acquired using DP Controller 2002 (Olympus) and processed using Adobe Photoshop version 5.5 (Adobe Systems, San Jose, CA, USA). Original magnifications: ×600 (A–J).

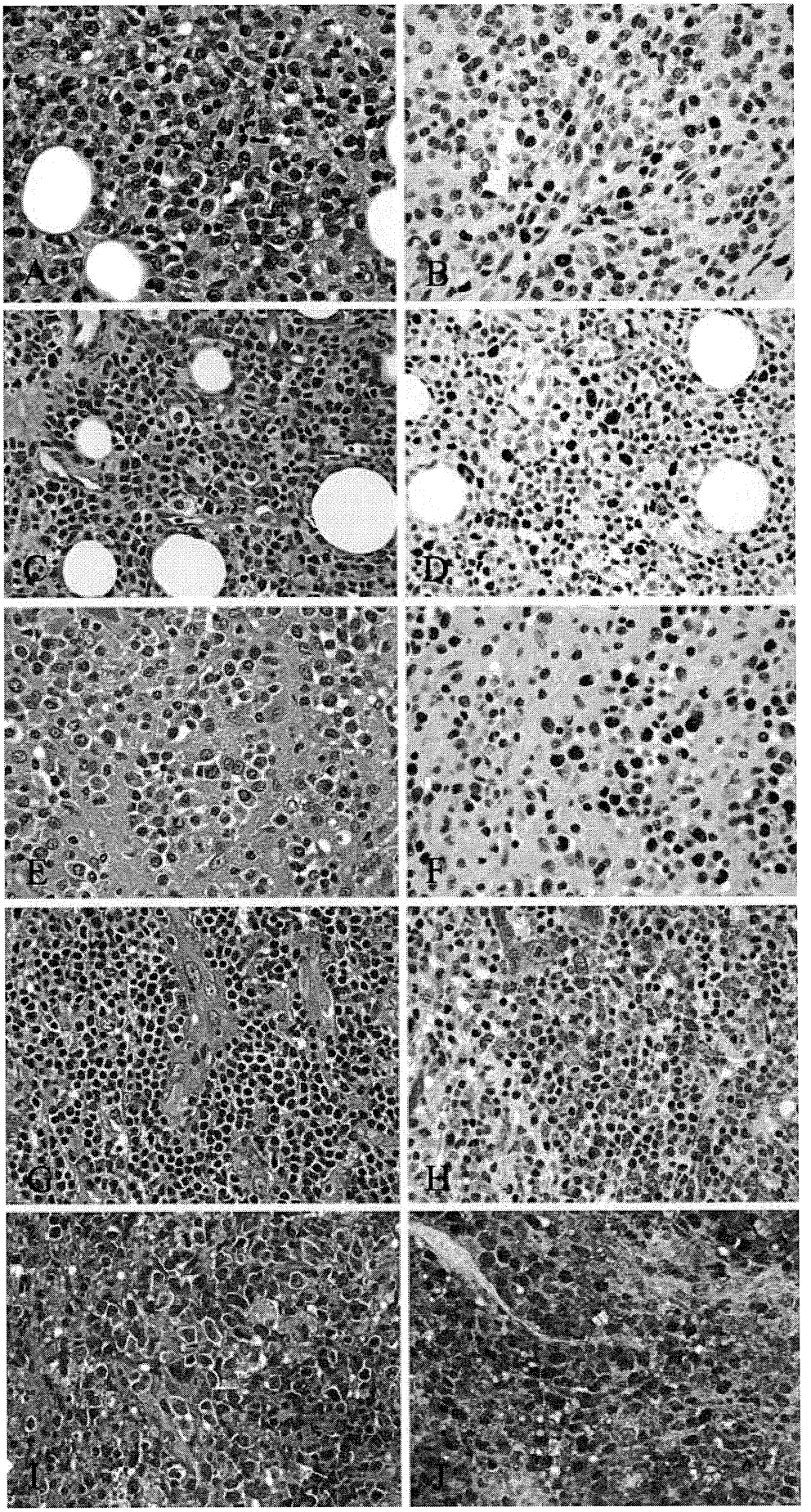

Figure 2.

J Pathol 2011; **223:** 496–510
www.thejournalofpathology.com

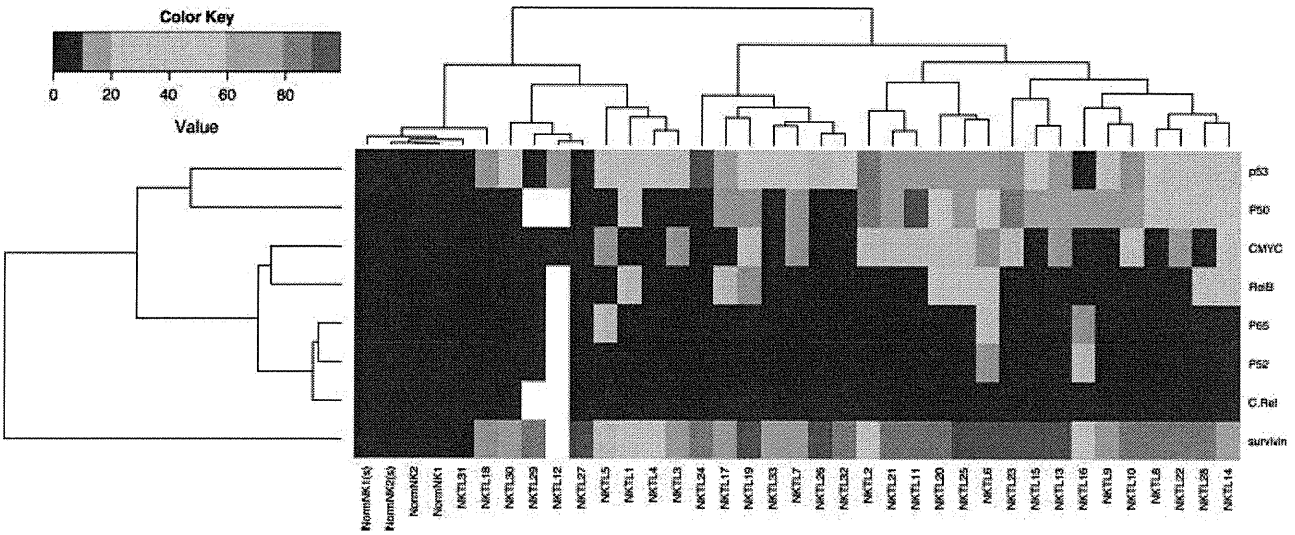

Figure 3. Clustering of samples based on expression of markers on IHC in NKTL (heat map). The samples used for IHC analysis were clustered based on the percentage of cells expressing the different markers used for IHC. Almost all cases of NKTL expressed aberrant p53 and survivin (not expressed in normal NK cells). Two main groups of NKTLs are defined by the expression pattern of these markers, with one group having c-Myc expression and stronger p50 expression, whereas the other only occasionally expresses c-Myc and p50. The legend for the colour coding in the heat map is shown to the upper left of the figure. 'White' indicates that tissue was not available for IHC staining of these markers.

MYC index (Supporting information, Supplementary Figure 4). Using FISH analysis, no break-apart signals were observed in 12 cases with adequate tumour cells and adequate hybridization, suggesting that MYC activation is not due to MYC rearrangements. In addition to p50, which is involved in the canonical NF-κB pathway, 27.3% (9 of 33) of NKTLs demonstrated positive expression for RelB, indicating that the non-canonical pathway may also be activated in a subset of NKTLs. In contrast, p52 and p65 were only infrequently expressed in 2 of 32 and 3 of 32 cases, respectively. None of our cases expressed c-Rel. Particularly striking was the immunoreactivity for survivin, where 29 out of the 32 positive cases (91%) showed expression in 50% or more of the tumour cell population, with strong staining in the majority of the cases. As expected, normal NK cells showed no expression or less than 10% expression for all the antibodies (Supporting information, Supplementary Table 8).

In order to study the relationship between the activation of Myc, p53, and NF-κB pathways and to determine whether there are distinct clusters based on the combination of these pathways, we clustered the samples according to the level of immunoreactivity for the different antigens (Figure 3). Almost all samples overexpressed p53 and survivin. Two main clusters were observed. The first, with hardly any expression of the markers tested, was clustered together with the normal NK cell samples. The second large cluster contained the remaining samples, with aberrant expression of one or more of these markers. Within the second cluster were two sub-clusters, one showing higher expression of p50 and c-Myc compared with the other. The clinical relevance of the different patterns of expression of these markers is not known as our sample size was small and there was no apparent difference in survival between these groups when we correlated the data with clinical outcome (data not shown).

Inhibition of survivin leads to apoptosis in NKTL cell lines

As survivin was aberrantly expressed in most of the NKTLs, we investigated whether inhibition of survivin would be therapeutically useful. We used western blot to assess the level of survivin protein expression in five NK cell lines (KHYG-1, NK-92, NK-YS, HANK-1, and SNK-6) and found overexpression of survivin in NK cell lines compared with normal NK cells, consistent with the IHC results (Figure 4A). The three cell lines with the highest survivin expression (KHYG-1, NK-92, and SNK-6) were selected for treatment with Terameprocol (EM-1421), a survivin inhibitor [21,22]. Successful suppression of survivin confirmed by western blot (Figure 4B) in KHYG-1 and NK92 resulted in a significant decrease in cell viability using the MTS assay (Figure 4C) and a dose-dependent increase in apoptosis compared with the control, as demonstrated in the bar chart (Figure 4D). In contrast, no significant change in cell viability or apoptosis in SNK-6 was observed when survivin was not suppressed by the inhibitor.

Discussion

NKTL is a relatively rare lymphoma that is highly aggressive, and current treatment strategies are clearly sub-optimal and chemoresistance is common [8,28]. A better understanding of the molecular abnormalities underlying this condition will provide important insights into the biology of this disease. In the past,

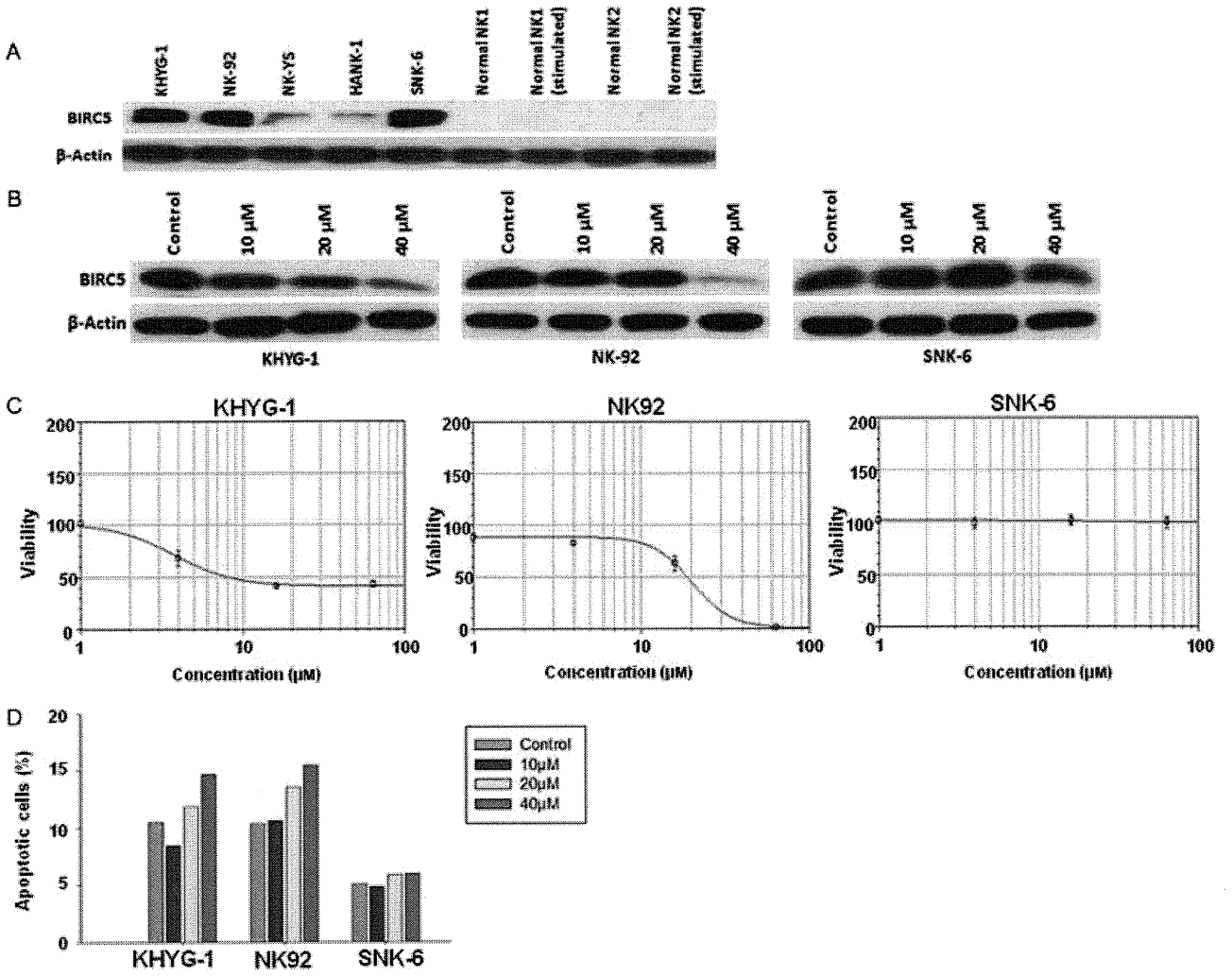

Figure 4. Inhibition of survivin leads to apoptosis in NK cell lines. Three NK cell lines with high expression of survivin (KHYG-1, NK-92, and SNK-6) identified by western blot (A) were treated with Terameprocol (survivin inhibitor) at 10, 20, and 40 μM or control for 48 h. There was successful dose-dependent inhibition of survivin in KHYG-1 and NK-92, confirmed by western blot with β-actin as the loading control (B). This was accompanied by a decrease in more than 50% of cell viability in the two cell lines and an increase in apoptosis detected by flow cytometry (C, D). The different concentrations of Terameprocol are represented by different colours according to the colour legend on the upper right of figure D. In contrast, there was no significant increase in apoptosis or decrease in cell viability in SNK-6 when survivin was not suppressed by the inhibitor.

it has been impossible to perform GEP using FFPE, due to RNA fragmentation. However, recent technology has enabled good-quality gene expression data to be obtained from FFPE samples [12]. We have shown in our study using a similar platform that we can obtain useful and meaningful GEP results from FFPE tissue. The validity of our results was supported by quantitative PCR validation as well as corroboration of our in silico functional analysis with immunohistochemistry in a larger TMA dataset, showing a good correlation between GEP, IHC, and western blot results. We did not attempt to categorize our cases into different clinical subtypes according to the site of involvement or cell of origin because of the small sample size.

Our results demonstrate a pro-proliferative and anti-apoptotic phenotype in NKTL, compared with normal NK cells, which is characterized by the activation of Myc and NF-κB, and deregulation of p53. NF-κB transcription factors are key regulators of immune, inflammatory, and acute phase responses [29] that have been implicated in oncogenesis through their transcription regulation of genes involved in cell cycle proliferation and cell adhesion, inhibition of apoptosis (including survivin) [30], and induction of cancer treatment resistance via the expression of multi-drug resistance-1 in tumour cells [30]. Among lymphoid malignancies, activation of NF-κB has been reported in mycosis fungoides [31], classical Hodgkin lymphoma, anaplastic large cell lymphoma, and peripheral T-cell lymphoma [32]. In NKTL, Liu *et al* [13] observed activation of NF-κB through the non-canonical pathway in 65.2% of NKTLs in China, and these cases were associated with chemoresistance and poor prognosis. NF-κB activation has also been shown in NK cell lines, and treatment of tumour cells with NF-κB inhibitors (BAY 11–7082 and curcumin) resulted in the suppression of NF-κB activation and induction of apoptosis [33]. Our data indicate

that the majority of cases showed activation of canonical NF-κB pathways through overexpression of p50, whereas only about 27% also concurrently engaged the non-canonical pathway. Our study therefore provides further evidence for the importance of NF-κB in NKTL, in line with the recent report by Huang *et al* [11].

Mutations of p53 resulting in overexpression of the protein have been demonstrated in a significant proportion of NKTLs [4,34]. Our data are not only consistent with these previous studies but further suggest that p53 deregulation is very common in NKTL. While abnormalities in p53 and NF-κB signalling have been reported in NKTL, Myc activation has not been previously described. The deregulation of these pathways in NKTL may explain the aggressive behaviour and relative drug resistance of these tumours [8,28]. It may also explain the efficacy of Velcade, which acts partly through targeting the NF-κB pathway [35].

While deregulation of p53 by mutations is described in NKTL, events mediating the activation of NF-κB and Myc pathways are unknown. We did not find any rearrangements in the *MYC* locus by FISH, suggesting that the activation of Myc in NKTL may be via *trans* mechanisms. A search of published data on NKTL revealed that abnormalities of DNA regions containing the genomic loci of the different NF-κB genes have not been described, indicating that the activation of NF-κB in NKTL is unlikely to be attributed to chromosomal alterations [10]. It may be possible that the constitutive activation of this pathway is the result of mutations in the NF-κB pathways, as was recently reported in lymphomas and myelomas [36,37].

As c-Myc is a transcriptional target of the EBV proteins EBNA2 [38] and LMP1 [39], and LMP1 is essential for EBV-mediated lymphocyte transformation by aggregating cellular proteins of the tumour necrosis factor receptor signalling pathway to activate NF-κB [40], it is possible that the activation of Myc and NF-κB in NKTL could be through the activity of EBV-related protein. This would be consistent with the importance of EBV infection in the pathogenesis of NKTL. Indeed, in EBV-immortalized B cells showing a latency III pattern, c-Myc and NF-κB are the two main transcriptional systems that are activated [41]. It is interesting to postulate that since EBV in NKTL shows a latency II pattern and lacks expression of EBNA-2 [2,3], the activation of c-Myc and NF-κB may be mediated primarily through LMP-1.

In this study, we observed remarkable overexpression of survivin in 97% of the NKTL samples. Survivin belongs to a family of human inhibitors of apoptosis and functions to counteract cell death by inhibiting caspase-9 activity and the intrinsic pathway of apoptosis [42]. Overexpression of survivin has been reported in many cancers, including some lymphomas, but has not been described in NKTL. In lymphomas, overexpression of survivin is associated with aggressive subtypes and inferior outcome [42,43]. Survivin is one of the target genes of NF-κB [30]. In addition, p53

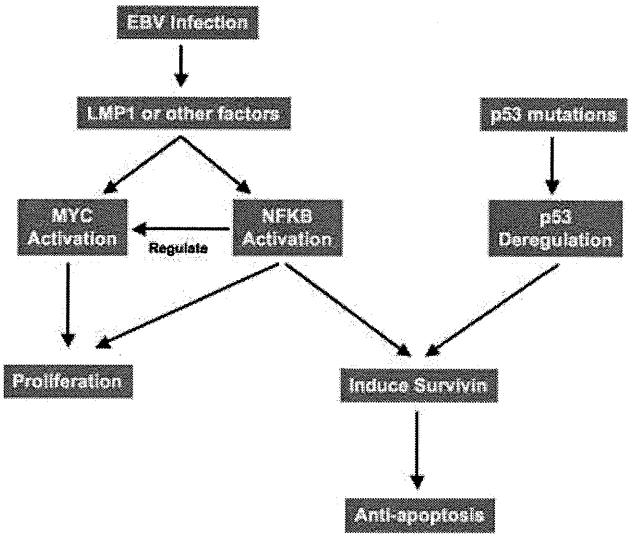

Figure 5. Model of NKTL pathogenesis involving the activation of Myc and NF-κB pathways, possibly driven by the EBV LMP-1 protein and/or other factors. In addition, the tumour acquires p53 mutations that lead to deregulated p53 function. The cumulative consequence of these oncogenic pathways results in proliferation and up-regulation of survivin, which leads to an anti-apoptotic effect on tumour cells.

deregulation can also contribute to the up-regulation of survivin, as demonstrated in melanoma [44], acute lymphoblastic leukaemia, and hepatocellular carcinoma. Therefore, the almost universal expression of survivin in NKTL is possibly downstream of p53 deregulation and/or NF-κB activation, which was observed in almost all of our cases of NKTL.

Based on our findings, we propose a model of NKTL pathogenesis involving the activation of Myc and NF-κB pathways, possibly driven by the EBV LMP-1 protein (Figure 5). In addition, the tumour acquires p53 mutations that lead to deregulated p53 function. The cumulative consequence of these oncogenic pathways is the up-regulation of survivin. The impact of Myc, NF-κB, and p53 pathways on the clinical outcome of our cases is not known as our sample size was small and there was no apparent difference in survival between these groups when we correlated the data with clinical outcome (data not shown). Furthermore, as these pathways are activated in most patients, they are more likely to play a central role in pathogenesis rather than having prognostic value. Our model does not exclude the participation of other pathways in NKTL pathogenesis. Recent studies showed that activation of the STAT3 pathway is common in NKTL [11]. In our analysis, STAT3 was one of the enriched transcription factors for genes differentially expressed between NKTL and normal NK cells, although the enrichment was much weaker than Myc, p53, and NF-κB (Table 2). Of interest, survivin is also one of the downstream targets of STAT3 [45].

Positive regulatory domain I (*PRDM1*) is another gene implicated in the biology of T-cell lymphomas. Zhao *et al* recently reported that PRDM1 transcripts were detected in T- and NK-cell lymphomas and

PRDM1 is involved in the chemoresistance of T-cell lymphomas [46]. In corroboration with this study, our GEP data revealed an up-regulation (2.5-fold) of PRDM1 in NKTL compared with normal NK cells (see Supporting information, Supplementary Table 6). As PRDM1 is a downstream target of NF-κB and *c-MYC* is a PRDM1-targeted gene [47,48], it is interesting to postulate that the activation of NF-κB may result in the up-regulation of PRDM1 and c-MYC in NKTL. Although these pathways may not be functional in all cases of NKTL, due to tumour heterogeneity, and they may not be the only important pathways activated, they are likely to represent key events during NKTL oncogenesis. This would fit with the current clinical phenotype of NKTL, being an aggressive tumour which is largely chemoresistant and universally associated with EBV infection.

Our results also suggest that survivin may represent a useful and novel therapeutic target in NKTL. Indeed, our *in vitro* studies using a survivin inhibitor, Terameprocol, showed that successful down-regulation of survivin in KHYG-1 and NK-92 cell lines led to a significant increase in apoptosis and a decrease in viability of the tumour cells. Terameprocol is a transcription inhibitor and it selectively reduces the transcription of genes that have promoters controlled by the Sp1 factor, such as survivin [49]. It is likely that pathways other than those controlled by Sp1, such as NF-κB, p53, and STAT3, also regulate the expression of survivin in NKTL and may account for the resistance of some of the NK cell lines, such as SNK-6, to Terameprocol treatment.

In conclusion, we have identified the activation of multiple oncogenic pathways in NKTL that leads to the almost universal overexpression of survivin. The deregulation of these pathways coupled with the high levels of survivin may explain the aggressive behaviour and relative resistance of NKTL to anti-cancer therapy. In line with this hypothesis are multiple studies reporting that overexpression of survivin in tumours confers resistance to a range of anti-cancer drugs [49]. Importantly, our data suggest the possibility of using survivin as a potential therapeutic target. Multiple strategies have been employed to target the function of survivin and although clinical trials targeting survivin for cancer treatment are still in their early development, initial results are promising [49].

Acknowledgment

We express our gratitude to Ms Choo Shoa Nian from the Department of Pathology, National University of Singapore, for performing immunohistochemistry. WJC is supported by an NMRC Clinician Scientist Investigator award. SBN is supported by a National University of Singapore start-up grant (R-179-000-040-133). This work was partly supported by a Singapore Cancer Syndicate Grant (SCS-GRN102). This material is based on research/work supported by the Singapore National Research Foundation and the Ministry of Education under the Research Centre of Excellence Programme.

Author contribution statement

SBN designed the study, performed immunohistochemistry and data analysis, and wrote the paper. VS performed experiments (GEP, PCR, and cell line survivin treatment) and wrote the paper. GFH performed the gene expression analysis and wrote the paper. JBZ performed the cell line survivin treatment. ALF and ML carried out the FISH analysis. YLK, NS, and YK contributed cell lines. AK designed the study and contributed cell lines. MS-T constructed TMAs and approved the paper. WJC designed the study, performed the gene expression analysis and data analysis, and wrote the paper.

References

1. Chan JKC, Quintanilla-Martinez L, Ferry JA, *et al*. Extranodal NK/T-cell lymphoma, nasal type. In *WHO Classification of Tumours of Haematopoietic and Lymphoid Tissues* (4th edn), Swerdlow SH, Campo E, Harris NL, *et al*. (eds). IARC Press: Lyon, 2008; 285–288.
2. Kanavaros P, Briere J, Emile JF, *et al*. Epstein–Barr virus in T and natural killer (NK) cell non-Hodgkin's lymphomas. *Leukemia* 1996; **10**(Suppl 2): s84–s87.
3. Xu ZG, Iwatsuki K, Oyama N, *et al*. The latency pattern of Epstein–Barr virus infection and viral IL-10 expression in cutaneous natural killer/T-cell lymphomas. *Br J Cancer* 2001; **84**: 920–925.
4. Quintanilla-Martinez L, Kremer M, Keller G, *et al*. p53 mutations in nasal natural killer/T-cell lymphoma from Mexico: association with large cell morphology and advanced disease. *Am J Pathol* 2001; **159**: 2095–2105.
5. Takahara M, Kishibe K, Bandoh N, *et al*. P53, N- and K-Ras, and beta-catenin gene mutations and prognostic factors in nasal NK/T-cell lymphoma from Hokkaido, Japan. *Hum Pathol* 2004; **35**: 86–95.
6. Takakuwa T, Dong Z, Nakatsuka S, *et al*. Frequent mutations of *Fas* gene in nasal NK/T cell lymphoma. *Oncogene* 2002; **21**: 4702–4705.
7. Yamaguchi M, Kita K, Miwa H, *et al*. Frequent expression of P-glycoprotein/MDR1 by nasal T-cell lymphoma cells. *Cancer* 1995; **76**: 2351–2356.
8. Bossard C, Belhadj K, Reyes F, *et al*. Expression of the granzyme B inhibitor PI9 predicts outcome in nasal NK/T-cell lymphoma: results of a Western series of 48 patients treated with first-line polychemotherapy within the Groupe d'Etude des Lymphomes de l'Adulte (GELA) trials. *Blood* 2007; **109**: 2183–2189.
9. Wong KF. Genetic changes in natural killer cell neoplasms. *Leuk Res* 2002; **26**: 977–978.
10. Iqbal J, Kucuk C, Deleeuw RJ, *et al*. Genomic analyses reveal global functional alterations that promote tumor growth and novel tumor suppressor genes in natural killer-cell malignancies. *Leukemia* 2009; **23**: 1139–1151.
11. Huang Y, de Reynies A, de Leval L, *et al*. Gene expression profiling identifies emerging oncogenic pathways operating in extranodal NK/T-cell lymphoma, nasal type. *Blood* 2010; **115**: 1226–1237.

12. Hoshida Y, Villanueva A, Kobayashi M, *et al*. Gene expression in fixed tissues and outcome in hepatocellular carcinoma. *N Engl J Med* 2008; **359**: 1995–2004.
13. Liu X, Wang B, Ma X, *et al*. NF-kappaB activation through the alternative pathway correlates with chemoresistance and poor survival in extranodal NK/T-cell lymphoma, nasal type. *Jpn J Clin Oncol* 2009; **39**: 418–424.
14. Drexler HG, Matsuo Y. Malignant hematopoietic cell lines: *in vitro* models for the study of natural killer cell leukemia–lymphoma. *Leukemia* 2000; **14**: 777–782.
15. Matsuo Y, Drexler HG. Immunoprofiling of cell lines derived from natural killer-cell and natural killer-like T-cell leukemia–lymphoma. *Leuk Res* 2003; **27**: 935–945.
16. Fan JB, Yeakley JM, Bibikova M, *et al*. A versatile assay for high-throughput gene expression profiling on universal array matrices. *Genome Res* 2004; **14**: 878–885.
17. Bibikova M, Talantov D, Chudin E, *et al*. Quantitative gene expression profiling in formalin-fixed, paraffin-embedded tissues using universal bead arrays. *Am J Pathol* 2004; **165**: 1799–1807.
18. Tusher VG, Tibshirani R, Chu G. Significance analysis of microarrays applied to the ionizing radiation response. *Proc Natl Acad Sci U S A* 2001; **98**: 5116–5121.
19. Ekins S, Nikolsky Y, Bugrim A, *et al*. Pathway mapping tools for analysis of high content data. *Methods Mol Biol* 2007; **356**: 319–350.
20. Remstein ED, Dogan A, Einerson RR, *et al*. The incidence and anatomic site specificity of chromosomal translocations in primary extranodal marginal zone B-cell lymphoma of mucosa-associated lymphoid tissue (MALT lymphoma) in North America. *Am J Surg Pathol* 2006; **30**: 1546–1553.
21. Ambrosini G, Adida C, Sirugo G, *et al*. Induction of apoptosis and inhibition of cell proliferation by *survivin* gene targeting. *J Biol Chem* 1998; **273**: 11177–11182. .
22. Chang CC, Heller JD, Kuo J, *et al*. Tetra-*O*-methyl nordihydroguaiaretic acid induces growth arrest and cellular apoptosis by inhibiting Cdc2 and survivin expression. *Proc Natl Acad Sci U S A* 2004; **101**: 13239–13244.
23. Marumoto T, Zhang D, Saya H, Aurora-A—a guardian of poles. *Nature Rev Cancer* 2005; **5**: 42–50.
24. Strebhardt K, Ullrich A. Targeting polo-like kinase 1 for cancer therapy. *Nature Rev Cancer* 2006; **6**: 321–330.
25. Malumbres M, Barbacid M, Cell cycle, CDKs and cancer: a changing paradigm. *Nature Rev Cancer* 2009; **9**: 153–166.
26. Annunziata CM, Davis RE, Demchenko Y, *et al*. Frequent engagement of the classical and alternative NF-kappaB pathways by diverse genetic abnormalities in multiple myeloma. *Cancer Cell* 2007; **12**: 115–130.
27. Huang G, Chng WJ. Predicting the oncogenic pathway activities of individual samples from microarray gene expression profiles. In *2009 International Workshop on Computational and Integrative Biology (CIB 2009)*, Hangzhou, China, 2009; 20–25.
28. Kwong YL. Natural killer-cell malignancies: diagnosis and treatment. *Leukemia* 2005; **19**: 2186–2194.
29. Li Q, Verma IM. NF-kappaB regulation in the immune system. *Nature Rev Immunol* 2002; **2**: 725–734.
30. Okamoto T, Sanda T, Asamitsu K. NF-kappa B signaling and carcinogenesis. *Curr Pharm Des* 2007; **13**: 447–462.
31. Izban KF, Ergin M, Qin JZ, *et al*. Constitutive expression of NF-kappa B is a characteristic feature of mycosis fungoides: implications for apoptosis resistance and pathogenesis. *Hum Pathol* 2000; **31**: 1482–1490.
32. Mathas S, Johrens K, Joos S, *et al*. Elevated NF-kappaB p50 complex formation and Bcl-3 expression in classical Hodgkin, anaplastic large-cell, and other peripheral T-cell lymphomas. *Blood* 2005; **106**: 4287–4293.
33. Kim K, Ryu K, Ko Y, *et al*. Effects of nuclear factor-kappaB inhibitors and its implication on natural killer T-cell lymphoma cells. *Br J Haematol* 2005; **131**: 59–66.
34. Li T, Hongyo T, Syaifudin M, *et al*. Mutations of the *p53* gene in nasal NK/T-cell lymphoma. *Lab Invest* 2000; **80**: 493–499.
35. Shen L, Au WY, Guo T, *et al*. Proteasome inhibitor bortezomib-induced apoptosis in natural killer (NK)-cell leukemia and lymphoma: an *in vitro* and *in vivo* preclinical evaluation. *Blood* 2007; **110**: 469–470.
36. Keats JJ, Fonseca R, Chesi M, *et al*. Promiscuous mutations activate the noncanonical NF-kappaB pathway in multiple myeloma. *Cancer Cell* 2007; **12**: 131–144.
37. Compagno M, Lim WK, Grunn A, *et al*. Mutations of multiple genes cause deregulation of NF-kappaB in diffuse large B-cell lymphoma. *Nature* 2009; **459**: 717–721.
38. Kaiser C, Laux G, Eick D, *et al*. The proto-oncogene c-*myc* is a direct target gene of Epstein–Barr virus nuclear antigen 2. *J Virol* 1999; **73**: 4481–4484.
39. Dirmeier U, Hoffmann R, Kilger E, *et al*. Latent membrane protein 1 of Epstein–Barr virus coordinately regulates proliferation with control of apoptosis. *Oncogene* 2005; **24**: 1711–1717.
40. Devergne O, Hatzivassiliou E, Izumi KM, *et al*. Association of TRAF1, TRAF2, and TRAF3 with an Epstein–Barr virus LMP1 domain important for B-lymphocyte transformation: role in NF-kappaB activation. *Mol Cell Biol* 1996; **16**: 7098–7108.
41. Faumont N, Durand-Panteix S, Schlee M, *et al*. c-Myc and Rel/NF-kappaB are the two master transcriptional systems activated in the latency III program of Epstein–Barr virus-immortalized B cells. *J Virol* 2009; **83**: 5014–5027.
42. Andersen MH, Svane IM, Becker JC, *et al*. The universal character of the tumor-associated antigen survivin. *Clin Cancer Res* 2007; **13**: 5991–5994.
43. Paydas S, Ergin M, Erdogan S, *et al*. Thrombospondin-1 (TSP-1) and survivin (S) expression in non-Hogkin's lymphomas. *Leuk Res* 2008; **32**: 243–250.
44. Raj D, Liu T, Samadashwily G, *et al*. Survivin repression by p53, Rb and E2F2 in normal human melanocytes. *Carcinogenesis* 2008; **29**: 194–201.
45. Zhou J, Bi C, Janakakumara JV, *et al*. Enhanced activation of STAT pathways and overexpression of survivin confer resistance to FLT3 inhibitors and could be therapeutic targets in AML. *Blood* 2009; **113**: 4052–4062.
46. Zhao WL, Liu YY, Zhang QL, *et al*. PRDM1 is involved in chemoresistance of T-cell lymphoma and down-regulated by the proteasome inhibitor. *Blood* 2008; **111**: 3867–3871.
47. Johnson K, Shapiro-Shelef M, Tunyaplin C, *et al*. Regulatory events in early and late B-cell differentiation. *Mol Immunol* 2005; **42**: 749–761.
48. Lin Y, Wong K, Calame K. Repression of c-myc transcription by Blimp-1, an inducer of terminal B cell differentiation. *Science* 1997; **276**: 596–599.
49. Ryan BM, O'Donovan N, Duffy MJ. Survivin: a new target for anti-cancer therapy. *Cancer Treat Rev* 2009; **35**: 553–562.

SUPPORTING INFORMATION ON THE INTERNET

The following supporting information may be found in the online version of this article.

Supplementary methods.

Table S1. Clinical data of nasal-type extranodal natural killer/T-cell lymphoma study cases.

Table S2. Immunohistochemistry: antibodies and staining conditions.

Table S3. Characteristics of cell lines derived from NK-cell neoplasm used in this study.

Table S4. Primers used for PCR validation.

Table S5. BAC clones used to prepare fluorescence *in situ* hybridization probes.

Table S6. Genes differentially expressed between NKTCL and normal NK cells.

Table S7. Summary of results for immunohistochemistry for c-Myc, p53, NF-κB proteins, and survivin in NKTL samples.

Table S8. Summary of results for immunohistochemistry for c-Myc, p53, NF-KB proteins, and survivin in normal NK cells.

Figure S1. Quantitative PCR validation of several candidate genes showed that on the whole this is consistent with gene expression data showing higher expression of EZH2, STMN1, and BIRC5 (survivin) in NKTL compared with unstimulated and stimulated normal NK cells.

Figure S2. A heat map of normalized iPASA scores.

Figure S3. Expression of leading contributing genes from the enriched metastasis related gene sets.

Figure S4. Comparison of gene expression-based MYC index with MYC staining by immunohistochemistry.

Lab on a Chip

View Online
Dynamic Article Links

Cite this: DOI: 10.1039/c0lc00519c

www.rsc.org/loc

TECHNICAL NOTE

Point-of-care testing system enabling 30 min detection of influenza genes†

Tomoteru Abe,[a] Yuji Segawa,[a] Hidetoshi Watanabe,[a] Tasuku Yotoriyama,[a] Shinichi Kai,[b] Akio Yasuda,[a] Norio Shimizu[c] and Naoko Tojo[d]

Received 19th October 2010, Accepted 7th January 2011
DOI: 10.1039/c0lc00519c

We developed a portable and easy-to-use nucleic acid amplification test (NAT) system for use in point-of-care testing (POCT). The system shows sensitivity that is sufficiently higher than that of the currently available rapid diagnostic kit and is comparable to that of real-time reverse transcription polymerase chain reaction (RT-PCR) for influenza testing.

Currently, a rapid diagnostic kit employing immuno-chromatography is used in the diagnosis of infectious diseases (*e.g.*, influenza) and is widely used as a point-of-care test (POCT) because of its convenience and rapidity. However, this testing method has low sensitivity (*e.g.*, 40–69% for detection of influenza A)[1] and does not provide genetic information (*e.g.*, virus subtype, drug resistance) about the clinical sample. Furthermore, although reverse transcription polymerase chain reaction (RT-PCR) is used as a nucleic acid amplification test (NAT),[2] it is only applied to clinically important specimens due to the complexity of the procedures and time requirements. Our rapid testing system is portable, easy-to-use, and will allow quicker and more appropriate treatment.

Our NAT system comprises a disposable chip with multiple reaction wells, a heater, an optical system to measure fluorescence and a control system (Fig. 1a). An indium tin oxide (ITO) thin film on glass is used as the heater and to accommodate a transparent optical system. The optical components, including LEDs for excitation of fluorescent dye, photo-diodes for detection of fluorescent signal and lenses for focusing and collimating, are positioned to correspond to each well, which contributes to the miniaturization of the system (Fig. 1b). The disposable chip has a glass–polydimethylsiloxane (PDMS)–glass microfluidic structure and nine interconnected 1 μL reaction wells (Fig. 2a). The PDMS structure is bonded to the upper and lower glass in a vacuum chamber at less than 0.01 atm to produce an internal pressure of both the channel and wells of approximately 0.01 atm, which eliminates the need for pumps and tubing for injection of sample solution (Fig. 2b). Using vacuum aspiration, a nasopharyngeal swab sample extracted in solution including SYBR Green I is injected by a disposable injector with a needle to an injection port in the PDMS layer and can be loaded to all reaction wells within 10 s. Sample contamination among chips is

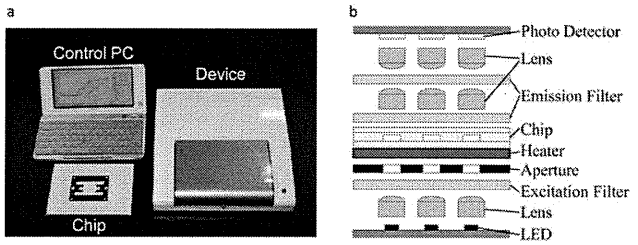

Fig. 1 POC NAT system and optical system. (a) The system includes a device for heating samples and detecting fluorescence, a laptop for controlling the system and disposable testing chips. (b) Cross-sectional view of the reaction and detection unit. Each well is equipped with a dedicated optical system: light from the LEDs is passed through a collimating lens directed to the sample, and excitation fluorescence is detected with photo-diodes.

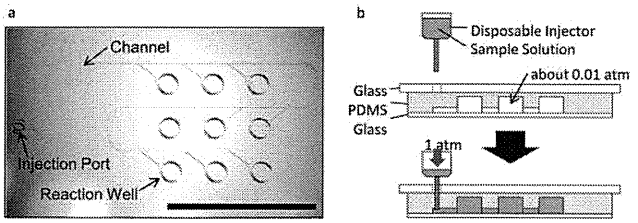

Fig. 2 The disposable testing chip. (a) The channel and reaction wells on the chip (scale bar = 1 cm). (b) Cross-sectional view of the disposable testing chip and conceptual diagram of sample injection. The interior pressure of both the channel and wells is maintained at approximately 0.01 atm. A sample solution can easily be loaded to the inlet of the chip and loads to all reaction wells within 10 s due to the vacuum aspiration. The self-sealing PDMS layer prevents fluid from escaping once the needle is removed.

[a]*Sony Corporation, Life Science Laboratory, Advanced Materials Laboratories, Tokyo Medical and Dental University, 1-5-45 Yushima, Bunkyo-ku, Tokyo, 113-8510, Japan*
[b]*Sony Corporation, Core Device Development Group, Life Electronics Business Development Department, 5-1-12 Kita-shinagawa, Shinagawa-ku, Tokyo, 141-0001, Japan*
[c]*Tokyo Medical and Dental University, Medical Research Institute, 1-5-45 Yushima, Bunkyo-ku, Tokyo, 113-8510, Japan*
[d]*Tokyo Medical and Dental University Hospital of Medicine, Department of Clinical Laboratory, 1-5-45 Yushima, Bunkyo-ku, Tokyo, 113-8510, Japan*

† Electronic supplementary information (ESI) available. See DOI: 10.1039/c0lc00519c

extremely unlikely because there is no outlet port. Loop-mediated isothermal amplification (LAMP), which has been reported to be a rapid, accurate and cost-effective method for diagnosing infectious diseases,[3,4] was adopted for nucleic acid amplification. The RNA amplification reagent (desiccant type) developed based on the LAMP method and primer sets for the influenza virus that have been commercialized for laboratory use were incorporated into our POC NAT system. The chip was prepared by aliquoting suitable quantities of primer mix (PM) and enzyme mix (EM) solutions (gifts from Eiken Chemical, Japan) for a 1 μL reaction to each well of the chip and desiccating these solutions. Thus, the chip has solid state reagents, avoiding the need for pipette work during analysis. As no purification of the clinical sample is necessary in this procedure, results can be obtained in 30 min.

In order to validate the practicability of our POC NAT system, we conducted two series of tests using clinical specimens. Seventy-seven patients (33 males and 44 females; mean age 33.4 years, range 3–89 years) with respiratory symptoms who visited the Tokyo Medical and Dental University Hospital outpatient clinic between December 2009 and February 2010 provided samples for these study. (Informed consent was obtained from these patients prior to sample collection.) First, we attempted to detect multiple genes on one chip (Fig. 3). We then used the residual solution of 45 nasopharyngeal swab samples from a rapid diagnostic test kit (ESPLINE Influenza A&B-N rapid diagnostic test kit: Fujirebio, Japan) to compare the POC NAT system and real-time RT-PCR detection. RNA from 140 μL of residual solution from the kit was purified by QIAamp Virus RNA Mini kit (QIAGEN, USA), and 3 μL of the purified RNA solution with Loopamp Extraction Reagent for Influenza Virus (EX) (Eiken Chemical, Japan) containing SYBR Green I was used to the POC NAT system containing EM with PM for human β-actin (ACTB) in wells 1–3, PM for H1pdm 2009 influenza (H1) in wells 4–6, and PM for influenza A (FluA) in wells 7–9. RT-PCR was conducted according to the WHO-recommended protocol[5] using 5 μL of the purified RNA solution. RT-PCR and the POC NAT system produced the same diagnostic results for 42 of 45 specimens. There were no false-positive results, indicating that there was no cross-contamination among the reaction wells (Table 1, ESI†). Next, we compared the sensitivities of RT-PCR and our NAT system and rapid diagnostic test kit. First, we suspended 42 nasopharyngeal swab samples in 130 μL of virus transfer medium (VTM: MEM medium base, including 0.5% BSA, 500 U mL^{-1} penicillin, 500 μg mL^{-1} streptomycin, 100 mg mL^{-1} gentamicin, and 2 μg mL^{-1} amphotericin B) and then suspended 40 μL of the VTM/sample suspension mixture in 4 mL of EX with SYBR Green I; 6 μL of this mixture was used to test the POC NAT system. Each well of the testing chips contained solid phase reagent: specifically, EM in all 9 wells, PM for H1 in wells 1–8, and ACTB in well 9. In parallel, 40 μL of the VTM/sample suspension mixture was resuspended in 2 mL of fresh VTM, and 140 μL of this solution was subjected to RT-PCR by the WHO-recommended protocol.[5] The POC NAT system successfully detected 20 out of 22 influenza-positive specimens, as determined by RT-PCR. Based on a total of 42 specimens tested (Table 1, ESI†), the sensitivity of our system is approximately 90.9% (20 of 22 RT-PCR positive samples). On the other hand, the sensitivity of rapid diagnostic test kit is estimated from the test results of the other swab samples from seventy-seven patients. In this study, we used the residual solution of 77 nasopharyngeal swab samples from a rapid diagnostic test kit (ESPLINE Influenza A&B-N rapid diagnostic test kit: Fujirebio, Japan) to compare the real-time RT-PCR detection. RNA from 140 μL of residual solution from the kit was purified by QIAamp Virus RNA Mini kit, and RT-PCR was conducted according to the WHO-recommended protocol[5] using 5 μL of the purified RNA solution. The sensitivity of the kit in our study is approximately 78.6% (33 of 42 RT-PCR positive samples).

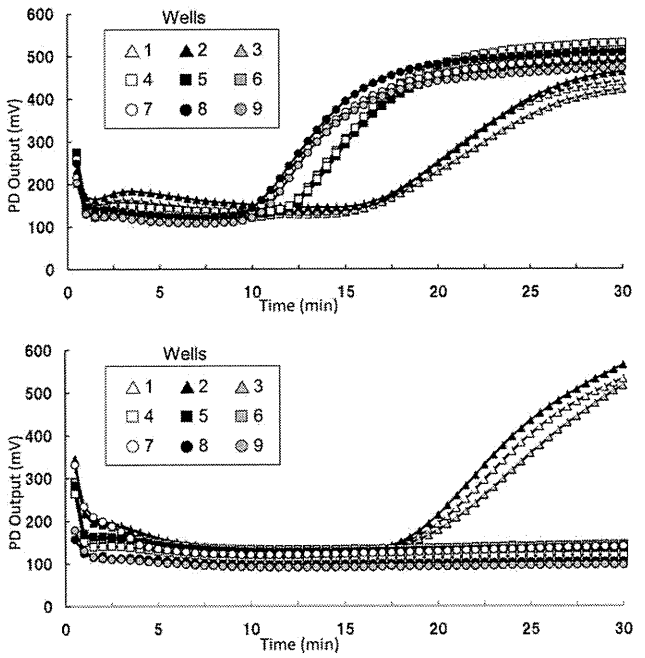

Fig. 3 Typical results from influenza testing for a positive result (upper panel) and a negative result (lower panel). The increase of output voltage indicates increased fluorescence corresponding to nucleic acid amplification. In the example shown, wells 1–3 were spotted with human β-actin primer, wells 4–6 were spotted primers specific to pandemic influenza and wells 7–9 were spotted consensus primers to influenza A.

We presented herein a POC NAT system that offers a solution to the problems associated with the commonly used rapid diagnosis kit and conventional NATs. Our POC NAT system is as easy to operate as the rapid diagnostic kit, and testing with the new system is completed in 30 min. Moreover, information regarding multiple genes can be obtained from a single test. Finally, the detection sensitivity of our POC NAT system is significantly higher than that of the rapid diagnostic kit and is comparable to that of RT-PCR. The technology utilized in the development of our NAT system will not only benefit current medical diagnostic procedures but will also be applicable to the detection of infectious diseases, such as tuberculosis and HIV, in developing countries that lack effective diagnostic procedures.

References

1 Centers for Disease Control and Prevention (CDC), *MMWR Morb. Mortal. Wkly. Rep.*, 2009, **58**, 826.
2 J. Versalovic and J. R. Lupski, *Trends Microbiol.*, 2002, **10**, S15.
3 T. Notomi, H. Okayama, H. Masubuchi, T. Yonekawa, K. Watanabe, N. Amino and T. Hase, *Nucleic Acids Res.*, 2000, **28**, E63.
4 Y. Mori and T. Notomi, *J. Infect. Chemother.*, 2009, **15**, 62.
5 World Health Organization, *WHO Information for Laboratory Diagnosis of Pandemic (H1N1) 2009 Virus in Humans—Revised*, World Health Organization, 23 November 2009.

Ann Hematol (2011) 90:851–852
DOI 10.1007/s00277-010-1095-x

LETTER TO THE EDITOR

Autoimmune hemolytic anemia and autoimmune neutropenia in a child with erythroblastopenia of childhood (TEC) caused by human herpesvirus-6 (HHV-6)

Hiroshi Yagasaki · Maiko Kato · Norio Shimizu · Hiroyuki Shichino · Motoaki Chin · Hideo Mugishima

Received: 20 September 2010 / Accepted: 23 September 2010 / Published online: 5 October 2010

Dear Editor,

Transient erythroblastopenia of childhood (TEC) is a self-limiting disorder of young children that is characterized by moderate to severe anemia with reticulocytopenia and decreased numbers of erythroid precursors in the bone marrow. TEC was often complicated with neutropenia and thrombocytopenia [1–3]. Here, we document a unique clinical course in a child with TEC.

A 1-year-old girl with anemia was admitted to our hospital. She had no recent episodes of viral infection such as fever and skin eruption. The values for hemoglobin (Hb) and reticulocytes were 57 g/L and 2.0% (Table 1). Although the direct Coombs test was highly positive, the haptoglobin level remained normal. In addition, the leukocyte fraction indicated agranulocytosis. Bone marrow findings were as follows: cellularity was normocellular, the erythroid series were reduced (M/E ratio, 4.2), and the myeloid series differentiated to a band form but not segmental neutrophils.

Speculating that viral infection was involved in this bicytopenia, we performed multiplex PCR analyses for the following viruses: herpes simplex virus type 1, type 2, human herpesvirus type 6 (HHV-6), type 7, type 8, varicella-zoster virus, Epstein-Barr virus (EBV), cytomegalovirus, parvovirus B19, polyomavirus JC, and polyomavirus BK, as described previously [4]. As a result, HHV-6 DNA (10×10^4 copies/μg DNA) was detected in the peripheral whole blood. Because we assumed that HHV-6 infection suppressed erythropoiesis, we started ganciclovir (GCV) from day 15. The reticulocyte count responded rapidly to GCV and increased to 10.8% on day 22 (Table 1). The HHV-6 DNA level also decreased significantly (0.84×10^4 copies/μg DNA); however, the Hb level decreased to 40 g/L on day 25.

As the haptoglobin level decreased, a diagnosis of hemolytic crisis was made. High-dose globulin (total dose, 1.5 g/kg) was given on days 25 to 27 with subsequent standard steroid therapy on days 37 to 74. The hemolysis resolved rapidly, and the Hb level increased up to 89 g/L on day 33. Coombs test became negative by day 67, and the patient was discharged on day 74. The level of HHV-6 antibody increased during this episode, which indicated a primary infection of HHV-6 (Table 1).

At present (day 273), the patient has no relapse of anemia. In contrast, the neutrophil count did not change. Anti-neutrophil antibodies were identified by flow cytometric analysis, which was consistent with autoimmune neutropenia.

The association between TEC and viral infection such as parvovirus B19, EBV, cytomegalovirus, and HHV-6 has been raised in few patients [5–7]. In our patient, HHV-6 infection was proven by a molecular technique and successfully treated using GCV. Another notable feature is that this patient presented with autoimmune hemolytic anemia and neutropenia, concurrently. We speculated that the immune response against HHV-6 has stimulated the production of multiple autoantibodies against red cells and

H. Yagasaki (✉) · M. Kato · H. Shichino · M. Chin · H. Mugishima
Department of Pediatrics, Nihon University,
Ohtaniguchi 30-1,
Itabashi-ku, Tokyo, Japan 173-8610
e-mail: yagasaki@med.nihon-u.ac.jp

N. Shimizu
Department of Virology, Medical Research Institute,
Tokyo Medical and Dental University,
Tokyo, Japan

Table 1 Laboratory results

	Normal range	Day 1[a]	Day 15	Day 22	Day 25	Day 33	Day 46	Day 67	Day 273
Hb (g/L)		57	52	47	40	89	91	108	122
Reticulocyte (%)		2	2.8	10.8	7.2	9	4.2	1.4	1.3
White blood cell (× 109/L)		4.6	7.5	3.1	4.4	4.7	6.2	5.8	5.3
Neutrophil (%)		0	0	0	0	2	0	0	2
Eosinophil (%)		1.5	0	1	2	0	0	4	1
Basophil (%)		0.5	0	0	0	0	0	1	0
Monocyte (%)		9	22	9	3	5	5	27	20
Lymphocyte (%)		85	77.5	90	95	93	94	68	77
Atypical lymphocyte (%)		4							
Platelet (× 109/L)		266	543	320	238	378	513	322	226
Total bilirubin (mg/dL)	0.3–1.2	0.5	0.62	1.32	0.65	0.93	0.36	0.35	0.21
Lactate dehydrogenase (U/L)	106–220	419	226	320	297	351	226	227	269
Coombs test (direct)		4+	4+	4+		3+	2+	–	–
Haptoglobin (mg/dL)	25–176	201	146		80	10	83	157	84
Erythropoietin (mU/mL)	8–36	1,460					86		
HHV-6 antibody (IgG)						<10	80	160	640

[a] Day 1 is the day of admission

neutrophils. Interestingly, marked hemolysis occurred just after the erythroid suppression was resolved. Because the structure and properties of the plasma membrane change extensively in the transition of reticulocytes into mature erythrocytes, the active target of hemolysis in this patient may be a molecule on reticulocytes rather than on mature red cells [8].

Conflicts of interest All authors have neither conflicts of interest nor financial support.

References

1. Hanada T, Koike K, Hirano C et al (1989) Childhood transient erythroblastopenia complicated by thrombocytopenia and neutropenia. Eur J Haematol 42:77–80
2. Rogers ZR, Bergstrom SK, Amylon M et al (1989) Reduced neutrophil counts in children with transient erythroblastopenia of childhood. J Pediatr 115:746–748
3. Cherrick I, Karayalcin G, Lanzkowsky P (1994) Transient erythroblastopenia of childhood. Prospective study of fifty patients. Am J Pediatr Hematol Oncol 16:320–324
4. Sugita S, Shimizu N, Watanabe K et al (2008) Use of multiplex PCR and real-time PCR to detect human herpes virus genome in ocular fluids of patients with uveitis. Br J Ophthalmol 92:928–932
5. Prassouli A, Papadakis V, Tsakris A et al (2005) Classic transient erythroblastopenia of childhood with human parvovirus B19 genome detection in the blood and bone marrow. J Pediatr Hematol Oncol 27:333–336
6. Penchansky L, Jordan JA (1997) Transient erythroblastopenia of childhood associated with human herpesvirus type 6, variant B. Am J Clin Pathol 108:127–132
7. Skeppner G, Kreuger A, Elinder G (2002) Transient erythroblastopenia of childhood: prospective study of 10 patients with special reference to viral infections. J Pediatr Hematol Oncol 24:294–298
8. Liu J, Guo X, Mohandas N et al (2010) Membrane remodeling during reticulocyte maturation. Blood 115:2021–2027

Leukemia (2011) 25, 1324–1334

www.nature.com/leu

ORIGINAL ARTICLE

The role of microRNA-150 as a tumor suppressor in malignant lymphoma

A Watanabe[1,6], H Tagawa[1,6], J Yamashita[2], K Teshima[1], M Nara[1], K Iwamoto[1], M Kume[3], Y Kameoka[1], N Takahashi[1], T Nakagawa[4], N Shimizu[5] and K Sawada[1]

[1]*Department of Hematology, Nephrology and Rheumatology, Akita University Graduate School of Medicine, Akita, Japan;* [2]*Radioisotope Research Laboratory, Bioscience Education-Reserch Center, Akita University, Akita, Japan;* [3]*Department of Internal Medicine, Hiraka General Hospital, Akita, Japan;* [4]*Department of Surgery, Senboku Kumiai General Hospital, Akita, Japan and* [5]*Division of Virology and Immunology, Medical Research Institute, Tokyo Medical and Dental University, Tokyo, Japan*

MicroRNA (miRNA; miR) is a class of small regulatory RNA molecules, the aberrant expression of which can lead to the development of cancer. We recently reported that overexpression of miR-21 and/or miR-155 leads to activation of the phosphoinositide 3-kinase (PI3K)–AKT pathway in malignant lymphomas expressing CD3$^-$CD56$^+$ natural killer (NK) cell antigen. Through expression analysis, we show in this study that in both NK/T-cell lymphoma lines and samples of primary lymphoma, levels of miR-150 expression are significantly lower than in normal NK cells. To examine its role in lymphomagenesis, we transduced miR-150 into NK/T-cell lymphoma cells, which increased the incidence of apoptosis and reduced cell proliferation. Moreover, the miR-150 transductants appeared senescent and showed lower telomerase activity, resulting in shortened telomeric DNA. We also found that miR-150 directly downregulated expression of *DKC1* and *AKT2*, reduced levels of phosphorylated AKT$^{ser473/4}$ and increased levels of tumor suppressors such as Bim and p53. Collectively, these results suggest that miR-150 functions as a tumor suppressor, and that its aberrant downregulation induces continuous activation of the PI3K–AKT pathway, leading to telomerase activation and immortalization of cancer cells. These findings provide new insight into the pathogenesis of malignant lymphoma.
Leukemia (2011) **25,** 1324–1334; doi:10.1038/leu.2011.81; published online 19 April 2011
Keywords: miR-150; microRNA; malignant lymphoma; NK/T-cell lymphoma; AKT2; senescence

Introduction

The genes responsible for T-cell and natural killer (NK)-cell lymphoma/leukemia are largely unknown because specific translocations have not yet been identified, although analyses to determine genomic copy number alterations revealed a 6q21 deletion, which is seen in about 10–20% of T and NK/T-cell lymphomas.[1–8]

Cancer cells gain a survival advantage by adding to abilities such as cell proliferation, anti-apoptotic function and immortalization. These changes are caused by altering the expression of oncogenes and/or tumor suppressor genes/proteins, such as c-Myc, Bcl2 and p53, among many others. In addition, recently discovered microRNAs (miRNAs) are known to associate with tumorigenesis and to alter the expression of both oncogenes and tumor suppressor genes.[9–12]

Correspondence: Dr H Tagawa, Department of Hematology, Nephrology and Rheumatology, Akita University Graduate School of Medicine, Akita 0108543, Japan.
E-mail: htagawa0279jp@yahoo.co.jp
[6]These authors contributed equally to this work.
Received 30 November 2010; revised 16 February 2011; accepted 15 March 2011; published online 19 April 2011

miRNAs are a class of small RNA molecules that have a regulatory function and have important roles in tumor development by pairing with the 3′-untranslated region (UTR) of target mRNAs to repress their productive translation.[9–12] Various miRNA alterations have been identified in lymphoma/leukemias, as well as in solid tumors, irrespective of the presence or absence of disease-specific genomic/genetic alterations.[9–12] We recently observed that two oncomiRs (miR-21 and miR-155) are overexpressed in NK/T-cell lymphoma, and that they contribute to lymphomagenesis by enhancing anti-apoptotic function. These miRNAs downregulate phosphatase and tensin homolog (PTEN), programmed cell death 4 and Src homology-2 domain-containing inositol 5-phosphatase 1 (SHIP1) while upregulating phosphorylated AKT$^{ser473/4}$.[13] These findings suggest that activation of the phosphoinositide 3-kinase (PI3K)–AKT pathway is important for NK/T-cell lymphomagenesis. Consistent with that idea, Huang *et al.*[14] recently used gene expression profiling to show the importance of activation of PI3K–AKT pathway in NK/T-cell lymphoma. Taken together, these results suggested miR-21 and miR-155 are upstream regulators of PI3K–AKT signaling.

In that context, the aim of the present study was to investigate the role of aberrantly downregulated miRNAs in T- and NK-cell lymphoma by using miRNA arrays, Northern blotting and quantitative PCR to examine miRNA expression in NK-cell and CD56$^+$ T-cell lymphoma lines. We found that expression of miR-150 is significantly diminished in both cell lines and in samples of primary lymphoma. We then tested the effects of transducing miR-150 to NK/T-cell lymphoma lines to determine whether it might function as a tumor suppressor.

Materials and methods

Lymphoma cell lines

NK and NK/T-cell lymphoma lines. We used 11 cell lines as NK/T-cell lymphoma leukemia cell lines, which are commonly showing CD2$^+$, sCD3$^-$, CD3ε$^+$, CD5$^-$, CD56$^+$, TCRαβ$^-$ and TCRγδ$^-$ phenotypes, including NKL, KHYG-1, YT, KAI-3, NK-92, HANK-1, SNK-1, SNK-6, DERL-7, SNK-10 and MOTN-1.[13–18] Of these, YT, KAI-3, HANK-1, SNK-1, SNK-6 and SNK-10 are EBV$^+$.[15,16] Although MOTN-1 was established from T-cell large granular lymphocyte leukemia, the cell line is showing NK-cell antigen.[17]

CD56$^+$ T-cell lymphoma lines. We also used five CD56$^+$ T-cell lymphoma lines including MTA, SNT-8, SNT-13, SNT-15 and SNT-16 cells, which are sCD3$^+$CD56$^+$ T-cell lymphoma cells showing T-cell receptor rearrangement.[18] MTA and

SNT-16 are TCR$\alpha\beta^+$, whereas the remaining cells are TCR$\gamma\delta^+$.[13] SNT-8, SNT-13, SNT-15 and SNT-16 cells are EBV$^+$.[18]

B-cell lymphoma cell lines. Raji and Daudi were derived from sporadic Burkitt lymphoma (EBV$^+$). Information of lymphoma cell lines used for this experiment is described in Supplementary Table 1.

Primary lymphoma samples and normal NK and T cells NK/T-cell lymphoma/leukemia. Nine samples of 'extra-nodal NK/T cell lymphoma, nasal type' and three samples of 'aggressive NK-cell leukemia' were collected from 12 patients. Out of 12 cases, 11 were previously used for miRNA analysis.[13] The remaining one case is described in Results section in this paper. These samples were positive for CD56, EBV infection or cytotoxic molecules such as TIA1 and GranzymeB. T cells showing the sCD3 ($n=15$) and NK cells showing the sCD3$^-$CD56$^+$ phenotype ($n=14$) were also collected from healthy donors using a magnetic cell sorting system (Miltenyi Biotec., Bergisch Gladbach, Germany)or cell sorter (Dako Cytomation MoFlo; Dako, Glostrup, Denmark). Polyclonal IL-2-activated NK cells were expanded in Iscove's modified Dulbecco's medium (Invitrogen, Carlsbad, CA, USA) supplemented with 10% human serum, 100 U/ml recombinant IL-2 (Hoffmann-La Roche, Basel, Switzerland) and 10% purified human IL-2 (Hemagen, Columbia, MD, USA). Resting NK cells were resuspended in the same medium without IL-2 and were used within 4 days after isolation. These cells were 95–99% CD3$^-$CD56$^+$, as determined by flow cytometry. All the samples were obtained from tumors at the time of diagnosis before any treatment was administered. Samples were obtained under protocol approved by the Institutional Review Board of Akita University.

miRNAs expression analyses

We performed miRNA array, Northern blot analysis and Taqman PCR analysis. Detail is described in Supplementary Methods. Ninety probes used for Northern blot and expression pattern of miRNAs are described in Supplementary Table 2.

Construction of plasmids and transduction

Lentiviral vectors for the delivery of miRNAs were designed and produced using the reagents and protocols included in the BLOCK-iT Lentiviral Pol II miR RNA interference expression system (Invitrogen). Detailed method is described in Supplementary Methods. The premicro-RNA (miR-150) inserted vector was transfected using Lipofectamine 2000 into 293FT producer cells. After overnight culture, the medium was replaced to remove the transfection reagents, and viral supernatants were collected the following day (72 h after transfection). Viral supernatants were applied to lymphoma cell lines. After removing the medium, the cells were cultured for an additional 48 h, and green fluorescent protein (GFP)$^+$ cells were collected using a cell sorter (Dako Cytomation MoFlo). In this study, we defined 'day 0' as the day on which lymphoma cells were sorted for GFP-miR-150 positivity: 48 h after either miR-150-GFP or GFP infection.

Antisense oligonucleotide assays

Antisense oligonucleotides (ASOs) and their respective scrambled control oligonucleotides were synthesized as hybrid deoxyribonucleotide molecules linked between the 2′-O and 4′-C-methylene bridge (locked nucleic acid) modification of G and C residues (Greiner, Tokyo, Japan) as described previously.[13,19]

Cell growth assay

Transduced cells (1.0×10^3/well, MOTN-1, SNK-6 and HANK-1) cultured in 96-well plates were transferred to 12-well plates, after which viable cells were identified by trypan blue exclusion and counted on days from 0 to 63 from miR-150 selection (at 2–65 days after transduction).

Cell proliferation assay (5′-bromo-2′-deoxyuridine assay)

Cell proliferation was assessed using a BrdU Cell Proliferation Assay kit (Merck, Darmstadt, Germany) following the manufacturer's protocol.

Apoptosis assay

An annexin V-PE apoptosis detection kit (BD Biosciences, San Jose, CA, USA) was used to assess the incidence of apoptosis among GFP$^+$ cells. Cells were exposed to 100 μM etoposide for 4 h, after which the assays were carried out.

Senescence-associated β-gal assay

Senescence-associated beta-gal was assayed using a Senescence Detection Kit (BioVision, Mountain View, CA, USA) according to the manufacturer's protocol.

Telomerase activity (telomeric repeat amplification protocol) assay

Telomerase activity was assayed using a $TRAP_{EZE}$ Gel-Based Telomerase Detection Kit (Millipore, Billerica, MA, USA). Cells (3×10^5) were suspended in CHAPS lysis buffer, and PCR was performed according the manufacturer's instructions.

Southern blot analysis

DNA (5 μg) was digested with *Hin*fI and transferred to Hybond N membranes (GE Healthcare Japan, Tokyo, Japan).

Western blot analysis

Antibodies against phospho-AKT$^{ser473/4}$ (pAKT), total AKT, AKT2 and c-Myc were all purchased from Cell Signaling Technology (Danvers, MA, USA; Cell Cycle Regulation Sampler Kit). Anti-p53 (DO-7) was from Dako Cytomation and anti-Bim (AAP-330) was from Stressgen Bioreagents (Funakoshi, Tokyo, Japan). Dyskerin (gene name: *DKC1*) was purchased from Santa Cruz Biotechnology (Santa Cruz, CA, USA).

Luciferase reporter assay

Double-stranded oligonucleotides corresponding to the wild-type (WT-3′-UTR) or mutant (MUT-3′-UTR) miR-150 binding site in the *DKC*1 of 3′-UTRs were synthesized (Sigma-Aldrich, St Louis, MO, USA) and ligated between the *Spe*I and *Hin*dIII restriction sites of the reporter plasmid pMIR-REPORT (Ambion, St Austin, TX, USA). 3′-UTR of mutated and wild-type AKT2 was amplified by PCR. Sequences of 3′-UTRs of the target genes of *DKC1* and *AKT2* are shown in Supplementary Table 3.

Results

Detection of candidate tumor suppressor miRNAs in NK/T-cell lymphomas

To identify aberrant expression of miRNAs in NK/T-cell lymphomas/leukemias, we initially carried out miRNA arrays with normal (sCD3$^-$CD56$^+$) NK cells and seven NK/T-cell lymphoma/leukemia lines (YT, KAI-3, KHYG-1, NKL, NK-92, HANK-1 and SNK-6). We found that expression of 37 out of 858 hsa-miRNAs was recurrently (two and more) reduced in the lymphoma cells, as compared with normal NK cells (Supplementary Table 2). To validate the expression of these miRNAs in NK/T-cell lymphomas/leukemias, we carried out Northern analyses with normal NK, T-cell and various lymphoma lines using 90 probe sets, which included candidate oncomiRs in various cancers (let-7, miR-15, miR-221 and so on),[10–12] as well as hematopoietic-specific miRNAs (miR-16, miR-451 and miR-223 and so on) (Supplementary Table 2).[20,21] The lymphoma cell lines used included those showing a sCD3$^-$CD56$^+$ phenotype (YT, KAI-3, NK-92, NKL, DERL-7, HANK-1, MOTN-1 and SNK-6), two T-cell lymphoma/leukemia lines (sCD3$^+$) (MyLa and JM) and two B-cell lymphoma lines (Raji and Daudi). Figure 1 shows the miRNA expression in four samples of normal/resting NK (sCD3$^-$CD56$^+$) cells and eight sCD3$^-$CD56$^+$ lymphoma lines. Northern analyses revealed that let-7e, miR-29c, miR-30e, miR-125a, miR-150, miR-181a and miR-223 were more highly expressed in NK cells than in the sCD3$^-$CD56$^+$ lymphoma cell lines. These differences were particularly evident in the case of miR-150 in NK-cell. For these candidate miRNAs, we also conducted Taqman quantitative PCR analysis using RNA collected from normal NK cells ($n=11$), NK/T-cell lymphoma/leukemia lines ($n=11$), and primary NK/T-cell lymphoma samples ($n=11$) (Supplementary Figure 1). This analysis confirmed that expression of miR-150, but not the other miRNAs tested, was significantly ($P<0.05$) higher in normal NK cells than in either the lymphoma cell lines or the primary lymphoma samples.

Aberrantly reduced expression of miR-150 in NK/T-cell lymphoma

Quantitative PCR revealed high levels of miR-150 expression in normal sCD3$^+$T, and sCD3$^-$CD56$^+$ NK cells. Figure 2a summarizes a set of quantitative PCR analyses carried out with NK cells (sCD3$^-$CD56$^+$) ($n=14$), T cells (sCD3$^+$) ($n=15$), NK/T-cell lymphoma lines (sCD3$^-$CD56$^+$TCR$^-$) ($n=11$) and CD56$^+$ T-cell lymphoma (sCD3$^+$CD56$^+$TCR$^+$) lines ($n=5$), as well as samples of primary NK/T-cell lymphoma/leukemia ($n=12$). We also compared expression of miR-150 in resting and activating NK cells and found that both the groups showed strong expression of miR-150, and that there was no significant difference between them (Figure 2b). The results show that the level of miR-150 expression in normal T and NK cells was significantly ($P<0.05$) higher than in the cell lines and primary lymphoma samples. For example, Northern analysis confirmed the reduced expression of miR-150 in a primary case of NK/T-cell lymphoma extranodal type (56-year-old female), showing positivity for pAKT, CD56, TIA-1 and EBV (Supplementary Figure 2). After collecting NK cells from the patient's peripheral blood, and taking tumor specimens from her nasal cavity, Northern analysis showed miR-150 expression to be markedly low than in normal NK cells. Notably, this patient showed no downregulation of miR-150 of her NK cells obtained from her peripheral blood, despite the CD56$^+$ phenotype of the tumor (Figure 2b). Figure 2c shows two cases of NK-cell lymphoma, extranodal type, representing very low expression of miR-150 when compared with normal NK cells.

Transduction of miR-150 into lymphoma lines and % GFP monitoring

To determine the role of miR-150 in the tumorigenesis of NK/T-cell lymphomas, we transduced miR-150 along with GFP into five NK/T-cell lymphoma cell lines (YT, KAI-3, MOTN-1, SNK-6 and HANK-1) and two B-cell lymphoma cell lines (Raji and Daudi). The transduction efficiencies were as follows: YT,

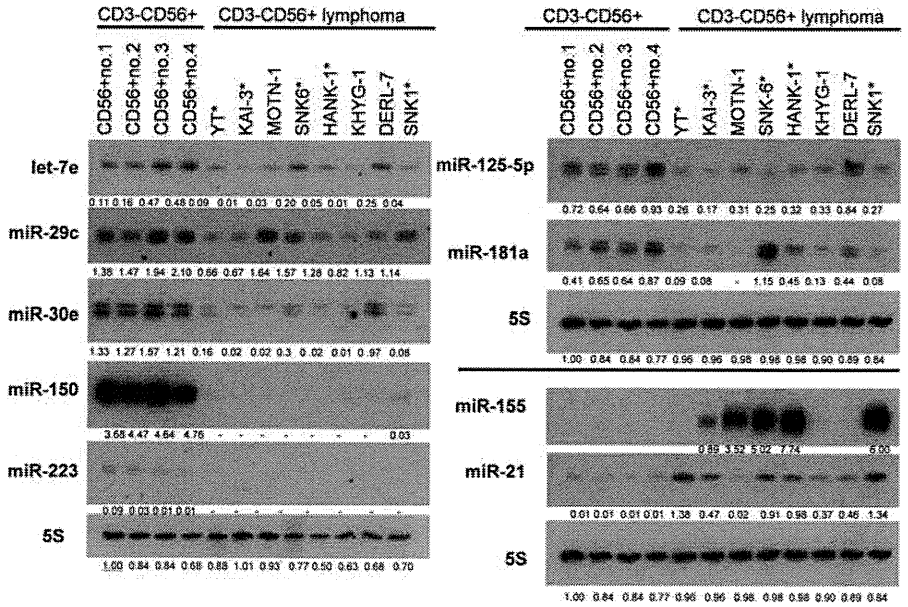

Figure 1 Expression analysis of downregulated miRNAs in NK/T-cell lymphoma/leukemia lines. Northern analysis of the expression of the indicated miRNAs in eight NK-cell lymphoma cell lines (sCD3$^-$CD56$^+$) and four samples of normal (sCD3$^-$CD56$^+$) NK cells. The cell types are indicated at the top. Fold changes in miRNA levels were determined by densitometry and are shown below the gels after normalization to the level of 5S RNA in normal NK cells (number 1), which was assigned a value of 1.00. Controls (5S tRNA) are shown below the miR-34a and miR-15a blots, respectively. Asterisks (*) indicate cell lines showing Epstein–Barr virus infection.